



Original article

Dynamic gut microbiome-metabolome in cationic bovine serum albumin induced experimental immune-complex glomerulonephritis and effect of losartan and mycophenolate mofetil on microbiota modulation



Wenyong Shi ^{a, b, 1}, Zhaojun Li ^{a, c, 1}, Weida Wang ^a, Xikun Liu ^a, Haijie Wu ^a,
Xiaoguang Chen ^a, Xunrong Zhou ^{d, **, *}, Sen Zhang ^{a, *}

^a State Key Laboratory of Bioactive Substances and Functions of Natural Medicines, Institute of Materia Medica, Chinese Academy of Medical Sciences & Peking Union Medical College, Beijing, 100050, China

^b State Key Laboratory of Functions and Applications of Medicinal Plants, College of Pharmacy, Guizhou Provincial Engineering Technology Research Center for Chemical Drug R&D, Guizhou Medical University, Guiyang, 550004, China

^c Department of Medicine Solna, Center for Molecular Medicine, Karolinska University Hospital and Karolinska Institute, Stockholm, 17176, Sweden

^d Department of Pharmacy, The Second Affiliated Hospital of Guizhou University of Traditional Chinese Medicine, Guiyang, 550001, China

ARTICLE INFO

Article history:

Received 14 August 2023

Received in revised form

14 December 2023

Accepted 28 December 2023

Available online 30 December 2023

Keywords:

Immune-complex glomerulonephritis

Gut microbiome

Metabolomics

Fecal microbiota transplant

Tryptophan metabolism

ABSTRACT

Dynamic changes in gut dysbiosis and metabolomic dysregulation are associated with immune-complex glomerulonephritis (ICGN). However, an in-depth study on this topic is currently lacking. Herein, we report an ICGN model to address this gap. ICGN was induced via the intravenous injection of cationized bovine serum albumin (c-BSA) into Sprague-Dawley (SD) rats for two weeks, after which mycophenolate mofetil (MMF) and losartan were administered orally. Two and six weeks after ICGN establishment, fecal samples were collected and 16S ribosomal DNA (rDNA) sequencing and untargeted metabolomic were conducted. Fecal microbiota transplantation (FMT) was conducted to determine whether gut normalization caused by MMF and losartan contributed to their renal protective effects. A gradual decline in microbial diversity and richness was accompanied by a loss of renal function. Approximately 18 genera were found to have significantly different relative abundances between the early and later stages, and *Marvinbryantia* and *Allobaculum* were markedly upregulated in both stages. Untargeted metabolomics indicated that the tryptophan metabolism was enhanced in ICGN, characterized by the overproduction of indole and kynurenic acid, while the serotonin pathway was reduced. Administration of losartan and MMF ameliorated microbial dysbiosis and reduced the accumulation of indoxyl conjugates in feces. FMT using feces from animals administered MMF and losartan improved gut dysbiosis by decreasing the *Firmicutes/Bacteroidetes* (F/B) ratio but did not improve renal function. These findings indicate that ICGN induces serous gut dysbiosis, wherein an altered tryptophan metabolism may contribute to its progression. MMF and losartan significantly reversed the gut microbial and metabolomic dysbiosis, which partially contributed to their renoprotective effects.

© 2023 The Author(s). Published by Elsevier B.V. on behalf of Xi'an Jiaotong University. This is an open access article under the CC BY-NC-ND license (<http://creativecommons.org/licenses/by-nc-nd/4.0/>).

1. Introduction

Immune-complex glomerulonephritis (ICGN) encompasses a variety of renal diseases characterized by immune-complex

deposition within glomeruli, including membranous nephropathy, lupus nephritis, IgA nephritis, and anti-glomerular basement membrane disease [1,2]. Dysbiosis of the gut microbiota promotes autoimmune disorders that damage extra-intestinal organs, including the kidneys, mainly through metabolism-dependent and immune-related pathways [3,4]. Recent findings suggest that the gut microbiota potentially acts as a primary mediator to enhance immune-complex deposition, complement activation, and inflammatory cell infiltration, leading to renal inflammation [5]. Gut dysbiosis can also cause intestinal metabolism dysfunction, leading

* Corresponding author.

** Corresponding author.

E-mail addresses: zhou168822@163.com (X. Zhou), zhangs@imm.ac.cn (S. Zhang).

¹ Both authors contributed equally to this work.

to increased production of various uremic toxins, including indoxyl sulfate (IS), p-cresyl sulfate (p-CS), trimethylamine, and trimethylamine *N*-oxide [6], which accelerates the progression of ICGN by intensifying inflammation [7]. Indole is a major catabolite of tryptophan produced by the gut microbiota, and other tryptophan-derived catabolites play different roles in intestinal health and ICGN progression [8]. A high-tryptophan diet induces autoimmune activation in lupus-prone mice mainly through the kynurenine-mediated downstream pathway [9]. Translocation of pathogens from the gut into circulation due to impaired gut barrier integrity in ICGN is another important factor that accelerates disease progression [10].

Despite an increase in the number of clinical studies on the role of the gut microbiota in chronic kidney disease (CKD), metagenome analyses, and animal experiments, studies specifically focusing on ICGN remain scarce, and most cases involve lupus nephritis and IgA nephritis. Different diseases have distinct features of gut microbiota alteration and metabolomics; therefore, there is a need to investigate the different characteristics of gut dysbiosis using different experimental ICGN models. An “idiopathic” rodent model of cationic bovine serum albumin (cBSA)-induced ICGN representing an autoimmune disease closely resembles human membranous nephropathy and provides a unique model with which to investigate the pathophysiological disease characteristics [11–13]. Therefore, in this study, c-BSA-induced ICGN was established and gut microbiota eubiosis, both in early and later stages, was investigated by sequencing the V3–V4 region of the 16S ribosomal DNA (rDNA) gene to determine which bacterial taxa contribute to the progression and deterioration of ICGN. Meanwhile, the metabolites in the feces were also examined via an untargeted high performance liquid chromatography-mass spectrometry (HPLC-MS) method, which aims to determine the relationship between altered metabolomics and gut microbiota dysbiosis and to identify the possible uremic toxins or metabolites derived from microbiota that participate in ICGN progression.

A deeper understanding of the gut microbiome-metabolome axis provides another alternative therapeutic strategy by manipulating the gut microbiota to treat disease and provides an alternative perspective to explain the efficiency of the drug. Immunosuppressive agents and angiotensin-converting enzyme inhibitors are most used drugs to treat ICGN in clinical practice, such as mycophenolate mofetil (MMF) and losartan [14,15]. MMF is a first-line immunosuppressive agent for the treatment of membranous glomerulonephritis that can block purine synthesis and selectively inhibit the proliferation of T and B lymphocytes [16]. Although the therapeutic target is not the gut microbiota, MMF has been reported to cause gastrointestinal adverse effects by reshaping the gut microbiota during transplantation [17]. Losartan has been widely used to treat CKD [18], and it has been shown to improve renal hemodynamics and renal vascular resistance. The benefits of losartan in the treatment of advanced immune nephropathy with impaired renal function have been reported [19], and a previous study suggested that changes in the gut microbiota induced by losartan contribute to its antihypertensive effects [20]. Although their renal beneficial effects are clear, whether these two drugs are able to reverse gut microbiota dysbiosis in ICGN requires further study, and whether the modulation of the gut microbiota contributes partially to their renal protective effect remains to be demonstrated. This study not only provides a comprehensive dynamic profile of gut microbiome-metabolomic changes in c-BSA-induced experimental ICGN, but also provides new perspectives regarding the beneficial effects of MMF and losartan from the perspective of modulating the gut microbiota.

2. Materials and methods

2.1. Experimental design and drug administration

C-BSA was prepared according to a previously described protocol [21–23]. Female Sprague-Dawley (SD) rats (180–200 g) were obtained from the Institute of Laboratory Animal Science, Chinese Academy of Medical Sciences, Beijing, China. Rats were maintained under a 12-h light/dark cycle at 25 °C and a humidity of 60% ± 10%. Animal experiments were performed in accordance with the institutional regulations on the use of experimental animals, which were approved by the Ethics Committee of Laboratory Animals of Peking Union Medical College (Beijing, China) (Approval No.: 003564; 2019). Experimental ICGN rats were established according to a previous protocol [21]. Briefly, rats were administered consecutive intravenous injections of c-BSA (5 mg per animal) (Biolead, Beijing, China) for two weeks. Albuminuria 10 times higher than the normal control suggested that ICGN was successfully established. The sham group ($n = 10$) received the same volume of phosphate-buffered solution (PBS) (Living, Beijing, China) intravenous injection. After two weeks, all albuminuric rats were randomly allocated to three groups: i) vehicle, ii) losartan (Merck, Hangzhou, Zhejiang, China), or iii) MMF ($n = 10$ for each group; Roche, Shanghai, China). Losartan and MMF were dissolved in 0.5% sodium carboxymethyl cellulose (CMC-Na) solution buffer (Shanghai Hushi Laboratories Equipment Co., Ltd., Shanghai, China) and orally administered to the animals each day for four consecutive weeks, while animals in the vehicle-treated group were administered the same volume of CMC-Na solution buffer. To maintain the albuminuria status of ICGN, the animals were administered c-BSA intravenously twice weekly during drug administration. The treatment period lasted for four weeks for Experiment 1, and a detailed procedure is provided in Fig. S1A. The objective of this experiment was two-fold: first, to verify altered intestinal microbiota and metabolites at the early and later stages of c-BSA-induced ICGN; and second, to evaluate the impact of losartan and MMF on the gut microbiota and further investigate whether their renal protective effect was partially derived from the modulation of the gut microbiota.

At the end of the experiment, after fasting for 18 h, the experimental animals were anaesthetized with 2.5 mL/kg equitensin, blood was collected from the retro-orbital sinus, and urine was collected through metabolic cages. Serum and urine biochemical parameters, including blood urine nitrogen (BUN), serum creatinine (Scr), triglyceride (TG), low-density lipoprotein, and high-density lipoprotein cholesterol, were examined using a Hitachi automatic analyzer (Tokyo, Japan). Albuminuria was assessed using an enzyme linked immunosorbent assay (ELISA) kit (Abcam, Cambridge, MA, USA). The serum lipopolysaccharide (LPS) levels were measured by ELISA using a luminometer (BioTek Instrument, Inc., Vermont, CA, USA) at 450 nm, according to the manufacturer's instructions. Before sacrificing, fecal samples were collected from each animal and processed for 16S rDNA sequencing and untargeted and targeted metabolomic analyses. Subsequently, all animals were sacrificed and feces, colon, and kidney tissues were collected [24].

2.2. Histological analysis

Partial kidney and colon tissues were fixed in 10% phosphate-buffered formalin and embedded in paraffin (Beijing Labgic Technology Co., Ltd., Beijing, China). Sections of 2- μ m thickness were cut and stained with hematoxylin and eosin (HE) and Masson. Two independent pathologists performed the histological assessments.

The glomerulosclerosis score was determined in the glomerular cross-sections using Masson staining and graded semi-

quantitatively on a scale of 0–4, where grade 0 indicates very weak or absent Masson staining, and grades 1–4 indicate focally strong staining in <25%, 25%–50%, 50%–75%, and 75%–100% of the glomerular area, respectively. Twenty randomly selected glomeruli were evaluated for each animal, and all fields for morphometric analysis were randomly selected. Tubulointerstitial damage (infiltration, protein cast, fibrosis, tubular dilatation, or atrophy) was evaluated semi-quantitatively, as in previous studies [5], in which grading was performed according to the extent of the damaged tubulointerstitial area in the renal cortex: grade 0, normal; grade 1, <10%; grade 2, 10%–25%; grade 3, 25%–50%; grade 4, 50%–75%; and grade 5, 75%–100%. The extent of damage was evaluated by visually selecting the injured areas in successive fields in the cortical and juxtamedullary areas of each biopsy.

Colon tissue damage was scored according to the following criteria [25]: 0, no damage; 1, lymphoepithelial lesions; 2, focal ulceration or surface mucosal erosion; and 3, broad mucosal damage involving the deeper structures of the intestinal wall. The inflammatory cell infiltration score was evaluated according to the following criteria [25]: 0, few inflammatory cells in the lamina propria; 1, increased infiltration of inflammatory cells into the lamina propria; 2, group of inflammatory cells infiltrating the submucosa; and 3, transmural infiltration of inflammatory cells. The histological score was determined by combining the scores for tissue damage and inflammatory cell infiltration. Each section was evaluated based on five randomly selected fields.

2.3. Immunofluorescence and immunohistochemistry

Immunohistochemical staining was performed as previously described [26]. Briefly, colon tissue sections were subjected to deparaffinization, hydration, and microwave antigen retrieval, followed by incubation at 37 °C for 45 min with primary antibody against cluster of differentiation 68 (CD68) and tumor necrosis factor- α (TNF- α) (1:100; Abcam). IgG deposition in the glomerular compartment was examined by immunofluorescence, as described previously [27]. An image analysis software (NDP Viewer 2; Hamamatsu Photonics, Tokyo, Japan) was used to further analyze the panoramic scanning images.

Staining of IgG and TNF- α was calculated quantitatively in terms of the staining distribution and optical density using Image-Pro-Plus software based on the five-point grading system. Random five fields were selected for each animal. CD68-positive cell infiltration was evaluated and expressed as positive cells per mm² in the colon tissue.

2.4. Electron microscopy

Transmission electron microscopy (TEM) was used to further investigate the colon ultrastructure. Briefly, ultrathin sections were prepared as previously described [14]. Small pieces of intestinal segments (1 mm \times 1 mm) were fixed in a 2.5% glutaraldehyde solution buffered with sodium cacodylate buffer (pH 7.4 for 2 h, post-fixed for 1 h in 1% osmium tetroxide solution at the same temperature and pH and dehydrated in ethanol) (Beijing Tong Guang Fine Chemicals Company, Beijing, China). After embedding, the sections were stained with uranyl acetate and lead citrate (Shanghai Hushi Laboratories Equipment Co., Ltd.). TEM (JEM-1400; JEOL USA, Inc., Peabody, MA, USA) was used for observation and photography. The ultrastructures of tight junctions and intestinal villi in the colon were observed and quantified.

2.5. Western blot analysis

Protein was extracted from colon tissues using a lysis buffer containing a cocktail of phosphatase and protease inhibitors,

according to the standard protocol. Primary antibodies against claudin-1, MUC2, zonula occludens-1 (ZO-1), occludin, and β -actin were purchased from Abcam, and Western blotting was performed according to the standard procedure.

2.6. Fecal DNA extraction and 16S rDNA gene sequencing

Fresh feces were collected from each animal at the same time, and genomic DNA was extracted using a E.Z.N.A.® Soil DNA Kit (Omega Bio-Tek, Norcross, GA, USA) according to manufacturer's protocols. The concentration and purity of the resulting DNA were determined using a NanoDrop spectrophotometer (ND-2000; Thermo Fisher Scientific Inc., Waltham, MA, USA). Qualified DNA samples were sent to Novogene Biotech (Tianjin, China) for 16S rDNA gene sequencing according to standard procedures. Operational units (OTUs) were clustered with 97% similarity cutoff using USEARCH UPARSE (<http://www.drive5.com/uparse/>) [28,29].

2.7. Fecal metabolome and identification of metabolic pathways

Metabolites in the feces were examined using untargeted metabolomics ultra-performance liquid chromatography-high-definition MS (UPLC-HDMS). Metabolomic procedures, including sample preparation, metabolite separation and detection, data preprocessing, and statistical analysis for metabolite identification, are briefly summarized below.

The samples were analyzed using a 2.1 mm \times 100 mm ACQUITY 1.8 μ m HSS T₃ using a Acquity™ UPLC system (Waters Corporation, Milford, MA, USA) equipped with a Xevo™ G2 QToF MS (Waters Corporation). The metabolomic procedure, including sample preparation, metabolite separation and detection, data preprocessing, and statistical analysis for metabolite identification, was performed following previously described protocols with minor modifications [30]. Chromatographic separation was carried out at 40 °C on an ACQUITY UPLC HSS T₃ column (2.1 mm \times 100 mm, 1.8 μ m). The mobile phase comprised water (A) and acetonitrile (B), each containing 0.1% formic acid. The optimized UPLC elution conditions were: 0–1.0 min, 1.0% B; 1.0–12.0 min, 1.0%–99.0% B; 12.0–14.0 min, 99.0%–1.0% B; and 14.0–15.0 min, 1.0% B. The flow rate was 0.40 mL/min. The autosampler was maintained at 4 °C. Each run was injected 1 μ L of the sample solution.

MS was performed using a Xevo G2 Q-TOF instrument (Waters Corporation) with a scan range of m/z 50–1200. In the positive electrospray mode, the capillary and cone voltages were set at 3 kV and 30 V, respectively. The desolvation gas was set to 600 L/h at a temperature of 450 °C, the cone gas was set to 50 L/h, and the source temperature was set to 110 °C. The mass spectrometer was operated in the W optics mode at 12,000 resolutions using a dynamic range extension. The data acquisition rate was set to 0.1 s, with a 0.014 s interscan delay. The collision energy ramp was 20–30 V. All analyses were performed using LockSpray software (https://www.waters.com/waters/library.htm?locale=en_US&lid=1545617) to ensure accuracy and reproducibility. Leucine-enkephalin was used as the lockmass at a concentration of 300 ng/mL and a flow rate of 5 μ L/min. Data were collected in continuum mode, the lockspray frequency was set to 10 s, and the data were averaged over 10 scans. All data acquisition and analyses were controlled using Waters MassLynx v4.1 software. The acquired mass data were imported into Prognosis QI and MarkerLynx XS within the Masslynx software for peak detection and alignment. The resultant data matrices were introduced into Ezinfo 2.0 software (Waters Corporation).

2.8. Fecal microbiota transplantation

To determine whether the modulation of the gut microbiota by losartan and MMF contributed to their renal protective effects, a fecal microbiota transplantation (FMT) experiment was performed in Experiment 2. Briefly, the fecal contents were freshly collected and pooled from individual rats in the sham, vehicle, losartan, and MMF groups at the end of Experiment 1 and 24 h after the last dose of losartan or MMF. Recipient SD rats were orally gavaged with 180–200 g of donor fecal contents and grouped into R-Sham, ICGN-vehicle (R-ICGN), ICGN-losartan-treated (R-Losartan), and ICGN-MMF (R-MMF) groups, with each group containing six animals. FMT was performed in recipient rats as previously described [31,32]. The fecal contents were diluted 1:20 in sterile PBS and centrifuged at 60 g for 5 min. The supernatant was aliquoted and stored at -80°C . Recipient rats were orally gavaged with donor fecal contents (1 mL) as described above. Seven days after FMT, the animals were administered an intravenous c-BSA challenge. To avoid rapid albuminuria induced by c-BSA, it was injected every two days for four weeks. After four weeks, blood and urine samples were collected for biochemical analyses. The detailed protocol is presented in Fig. S1B.

2.9. Statistical analysis

All continuous counting data are presented as the mean \pm standard deviation. The statistical significance of differences between groups was analyzed using one-way analysis of variance (ANOVA) followed by the Bonferroni test or Student's *t*-test if the data were normally distributed. Principal component analysis (PCoA) and orthogonal partial least squares-discriminant analysis (OPLS-DA) were performed using the Soft Independent Modeling of Class Analogy software (<https://www.sartorius.com/en/products/process-analytical-technology/data-analytics-software/mvda-software/simca>) to cluster the sample plots across groups. The differential abundances of genera and metabolites were determined using non-parametric tests, including the Wilcoxon rank-sum and Mann-Whitney *U* tests. A negative or positive correlation coefficient indicates the type of correlation between the variables. *P*-values were corrected for multiple comparisons using the Benjamini-Hochberg false discovery rate, and $P < 0.05$ was considered to be statistically significant.

3. Results

3.1. Gradual decline in renal function and renal beneficial effect of MMF and losartan

After consecutive intravenous challenges with c-BSA for two weeks, a significant increase in albuminuria was observed, as well as decreased body weight, demonstrating the successful establishment of experimental c-BSA-induced ICGN (Fig. 1A). BUN but not Scr, was found to increase significantly in the ICGN group. As for the index of lipid metabolism dysfunction, another typical characteristic of ICGN, serum cholesterol was significantly increased in ICGN, while TG remained stable compared to that in the sham group (Fig. 1A). HE staining suggested that the histopathological impairment was mild, although IgG staining in the glomerular area was visible at this early stage (Fig. 1B).

After the establishment of albuminuria, MMF and losartan were orally administered for a period of four weeks. As shown in Fig. 1C, renal function declined quickly thereafter, manifested by increased Scr and albuminuria and impaired histopathological impairment, which was comprised of tubular casts, glomerulosclerosis, tubular cell necrosis, and inflammatory cell infiltration (Figs. 1D and E). All

these negative parameters were partially reversed by MMF and losartan, as shown in Figs. 1C and D, suggesting that these two drugs had satisfactory renal protective effects on ICGN, which was consistent with their clinical efficiency. In this study, at a dosage of 20 mg/kg, the effectiveness of MMF was better than that of losartan.

3.2. Mild alteration of gut taxa in ICGN rats after two weeks of c-BSA administration

Two weeks after the intravenous injection of c-BSA, kidney injuries were observed at a relatively early stage in the experimental animals, based on unchanged Scr and mild histopathological changes (Figs. 1A and B). At present, studies on dynamic changes in the gut microbiota in the early stages of experimental ICGN are rare. Therefore, fecal samples from the sham and ICGN groups were collected at this stage, and 16S rDNA sequencing was performed ($n = 10$) to evaluate the composition of the gut microbiota. 16S rDNA sequencing identified 491 OTUs from 878,904 quality-filtered sequences in the ICGN and sham groups. Several α -diversity indices, including Chao1, Sobs, Shannon, and Simpson, were used to determine the ecological diversity within microbial community, while only sobs index was found to be significantly decreased in the ICGN group compared with the sham group (Fig. 2A). A significant difference was observed in terms of β -diversity (PCoA) based on the unweighted (Adonis, $P = 0.004$) but not weighted (Adonis, $P = 0.086$) UniFrac between the sham and ICGN groups (Fig. 2B).

The taxonomic distributions of bacteria from the 16S rDNA sequencing data at the phylum (top 10) (Fig. 2C) and genus levels (top 15) (Fig. 2D) between the ICGN and sham rats suggested that moderate dysbiosis of the gut microbiota occurred at this stage. At the phylum level, *Firmicutes* was the most prominent gut bacterial community, accounting for an average of 56.6% and 45.3% of the sequences in the sham and ICGN rats, respectively. *Bacteroidetes* represented the second-most dominant gut bacterial community, accounting for an average of 40.5% and 51.2% of the sequences in the sham and ICGN rats, respectively. The *Firmicutes/Bacteroidetes* (F/B) ratio did not differ significantly between the two groups, although the average F/B ratio in the ICGN group was slightly higher than that in the sham group (Fig. 2E). The linear discriminant analysis (LDA) effect size (LEfSe, version 1.0) and Wilcoxon rank-sum test were used to compare the gut microbiota in the sham and ICGN rats at different taxonomic levels; all the differential taxa are shown in Fig. 2F (LDA > 3 , $P < 0.05$). PICRUSt (version 1.1.3, http://picrust.github.io/picrust/tutorials/quality_control.html) analysis revealed that the functional metabolic pathways predicted by gut dysbiosis were less affected. At levels 1 and 2 Kyoto Encyclopedia of Genes and Genomes (KEGG) analysis, no significant differences were observed between the two groups (Figs. S2A and B). At level 3, vancomycin resistance, unsaturated fatty acids, and biofilm formation (*Escherichia coli* (*E. coli*)) were significantly reduced in the ICGN group, whereas pathways associated with type I diabetes mellitus and Alzheimer's disease were enriched in the ICGN group (Fig. S2C).

3.3. Dysbiosis of the gut microbiota in later stages of ICGN

After another four-week c-BSA challenge (twice per week), kidney function in the ICGN group declined significantly, and histopathology demonstrated serious impairments (Figs. 1C and D). At this point, fecal samples were collected from each rat in the sham and ICGN groups, and 16S rDNA sequencing was repeated. As shown in Fig. 3A, the Chao1 and richness indices both decreased significantly, suggesting that richness in the gut continued to decrease compared to that in the early stage. Meanwhile, the evenness characteristic of the Shannon index also decreased in the

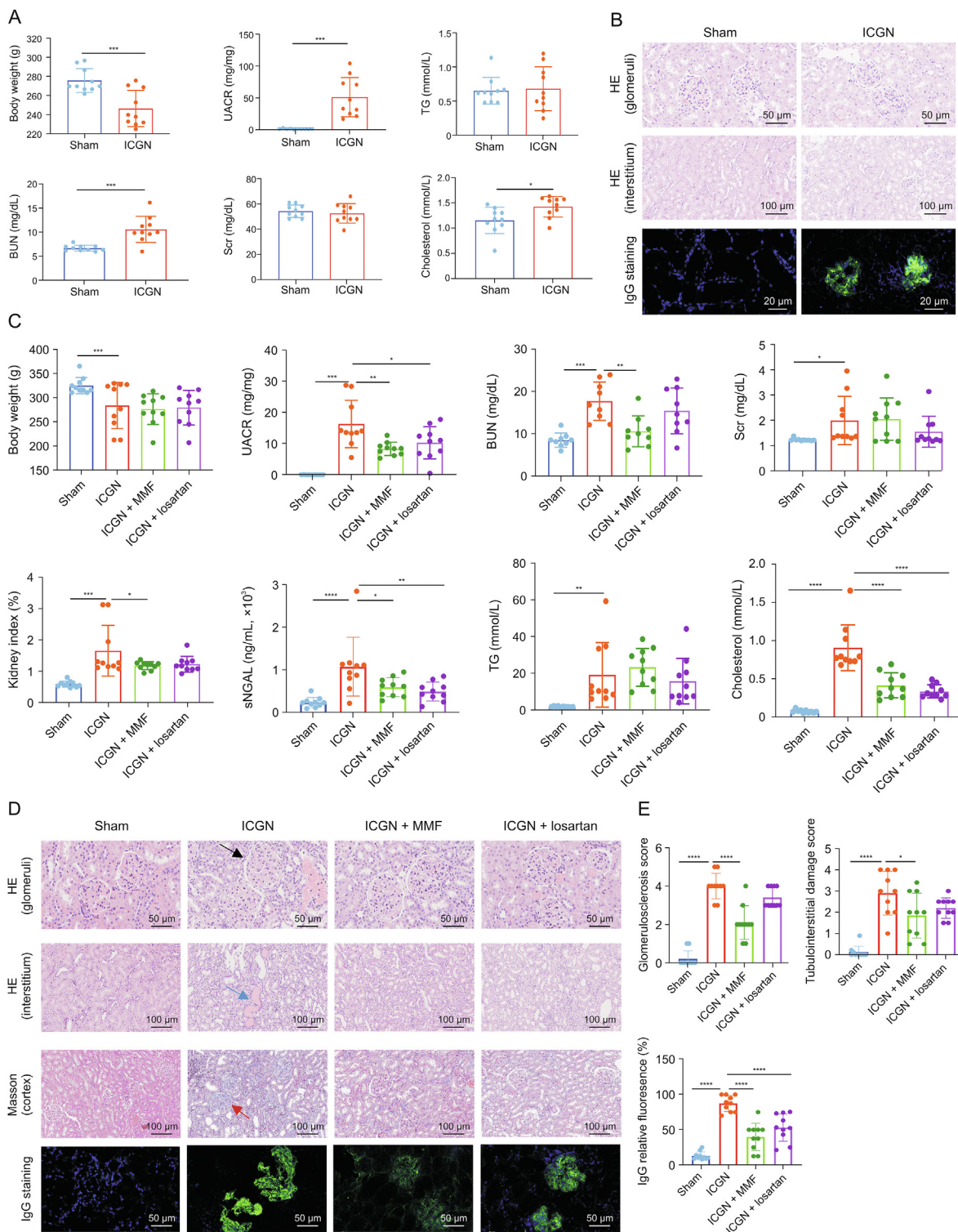


Fig. 1. Dynamic loss of renal function and histopathological injuries after six-week cationic bovine serum albumin (c-BSA) challenge between sham and immune-complex glomerulonephritis (ICGN) rats. (A) Changes in renal function after two weeks of c-BSA administration between sham and ICGN rats. (B) Glomerular and interstitial injuries by hematoxylin and eosin (HE) staining and IgG deposition in glomeruli by immunofluorescence after two weeks of c-BSA administration between sham and ICGN rats. (C) Renal function improved after the continuous oral administration of mycophenolate mofetil (MMF) and losartan for four weeks. (D) Glomerular and interstitial impairment by HE staining, cortex fibrosis by Masson staining, and IgG deposition in glomeruli by immunofluorescence after the continuous oral administration of MMF and losartan for four weeks, and their quantitation analysis. The black arrow indicates enlarged glomeruli (hypertrophy), the blue arrow indicates the protein cast, and the red arrow indicates fibrosis. * $P < 0.05$, ** $P < 0.01$, *** $P < 0.001$, and **** $P < 0.0001$ by analysis of variance (ANOVA) ($n = 10$). UACR: urine albumin-to-creatinine ratio; TG: triglyceride; BUN: blood urine nitrogen; Scr: serum creatinine; sNGAL: serum neutrophil gelatinase-associated lipocalin.

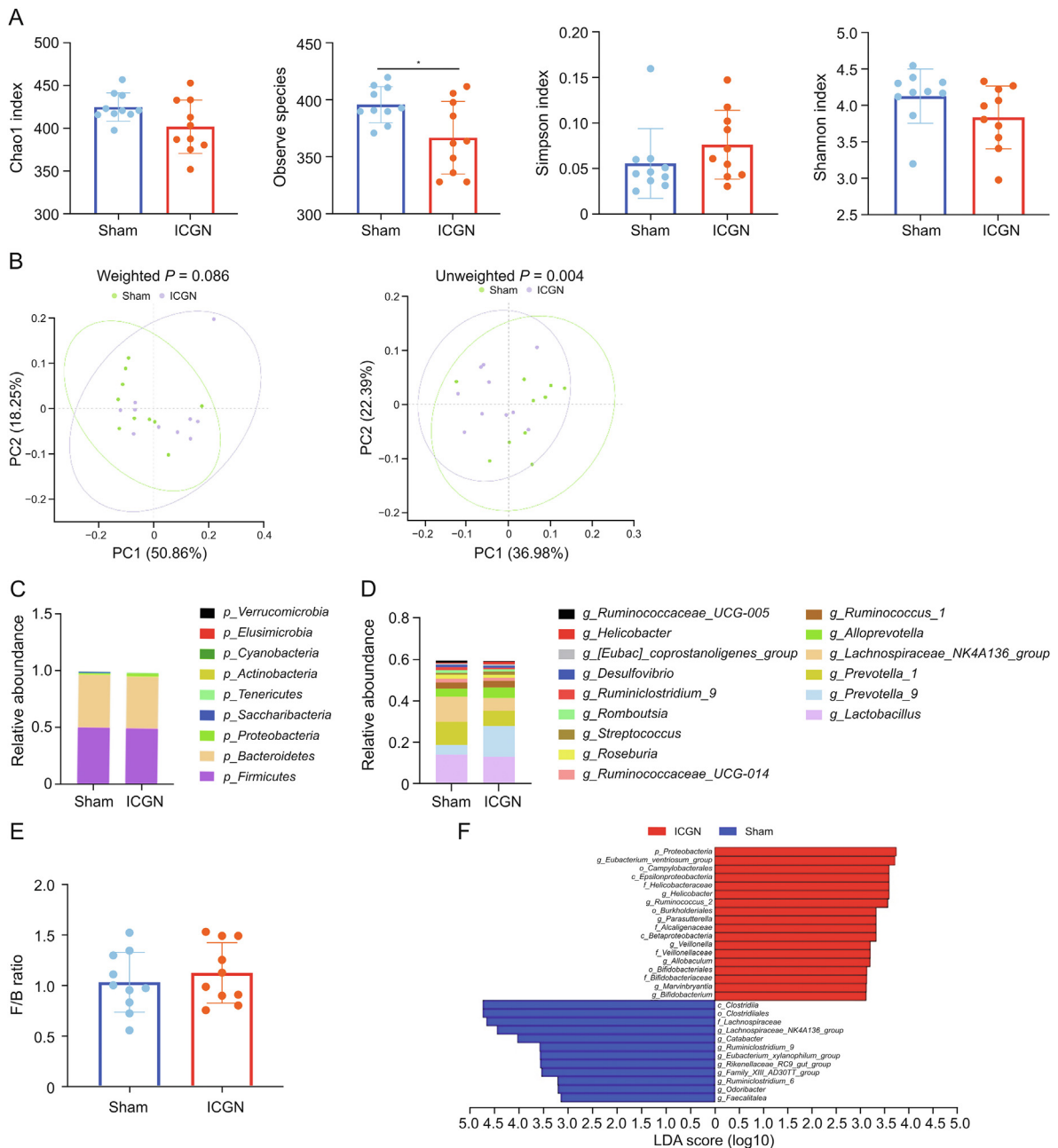


Fig. 2. Alteration of gut taxa in immune-complex glomerulonephritis (ICGN) rats after two weeks of cationic bovine serum albumin challenge. (A) Changes in α -diversity indices, including Chao1, observed species, Shannon, and Simpson index, between sham and ICGN rats. (B) A significant difference was observed in β -diversity (principal component analysis (PCoA)) based on the unweighted (Adonis, $P = 0.004$) but not weighted (Adonis, $P = 0.086$) UniFrac between the sham and ICGN rats. (C) Taxonomic distribution at phylum level between ICGN and sham rats by 16S ribosomal DNA (rDNA) sequencing. (D) Taxonomic distribution at the genus level between ICGN and sham rats by 16S rDNA sequencing. (E) The Firmicutes to Bacteroidetes (F/B) ratio at the phylum level. (F) Differential taxa of intestinal microbiota in sham and ICGN rats by linear discriminant analysis (LDA) effect size (LEfSe) analysis. * $P < 0.05$, ** $P < 0.01$, *** $P < 0.001$, **** $P < 0.0001$ by analysis of variance (ANOVA) ($n = 10$). PC: principal component.

ICGN group compared to that in the sham control ($P < 0.05$), although the Simpson index did not differ between these two groups. A significant difference was observed in terms of β -diversity (PCoA) based on both unweighted (Adonis, $P = 0.001$) and weighted (Adonis, $P = 0.008$) UniFrac between the sham and ICGN groups (Fig. 3B). Compared with the unweighted UniFrac difference at the early stage, these results suggest that dysbiosis of the gut microbiota was more severe than that at the two-week time point.

The relative abundance distribution at the phylum level is shown in Fig. 3C. In the ICGN group, the F/B ratio was found to

increase significantly at a later stage than in the sham group ($P < 0.05$). No significant difference was observed in the relative abundance of the major phyla, except *Tenericutes*, although its relative abundance was less than 1% in the whole fecal microbiota (0.75% in sham and 0.19% in ICGN, $P < 0.05$). The most abundant family was *Lachnospiraceae*. The relative abundance distribution at the family level is shown in Fig. 3D. In contrast to the early stage, the relative abundance of *Lachnospiraceae* in the ICGN group was significantly higher than that in the sham group. LEfSe analysis (LDA score > 3.0 , $P < 0.05$) showed all the differential taxa between the two groups, the number of which was significantly higher than that in the early

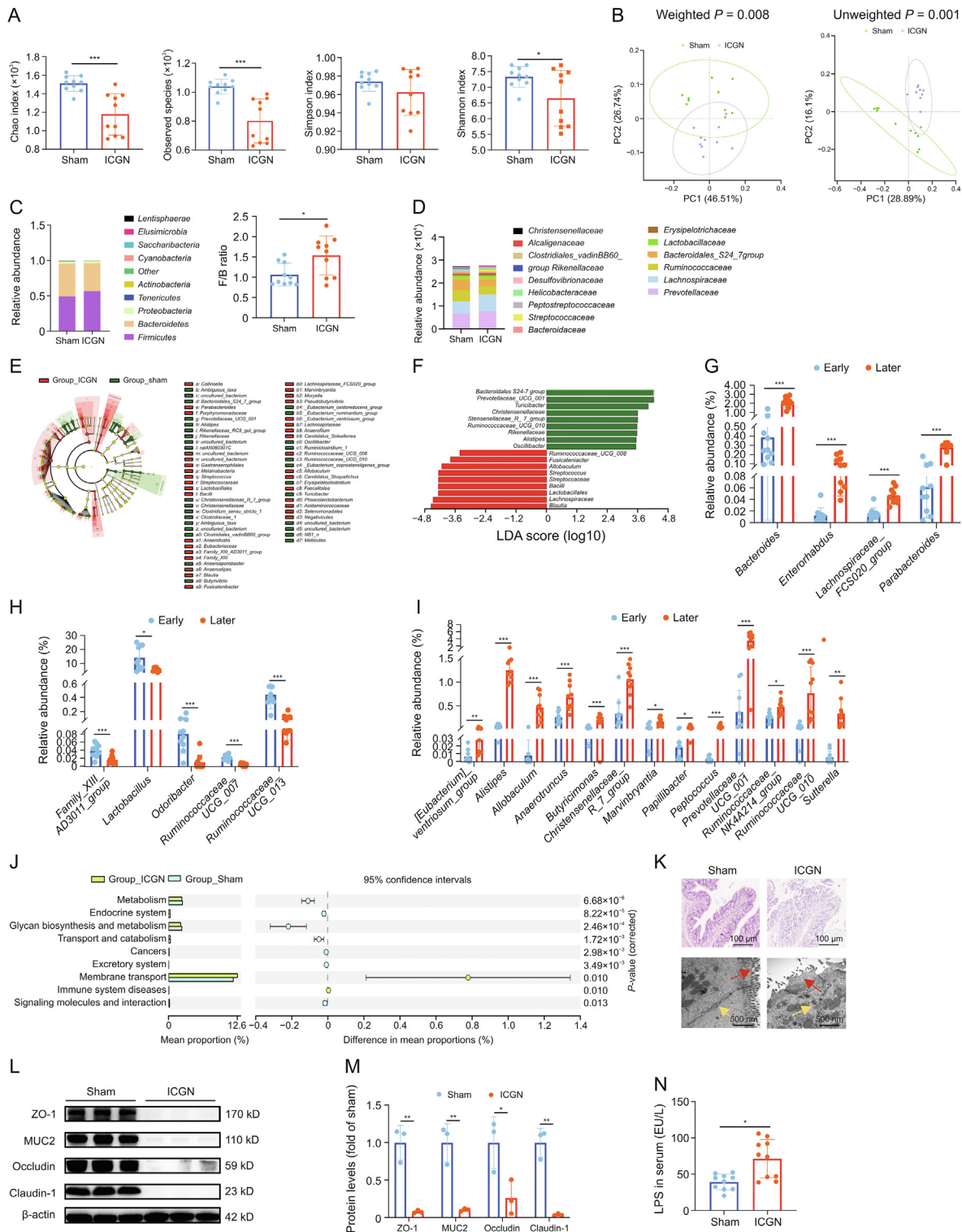


Fig. 3. Changes in the gut microbiota of immune-complex glomerulonephritis (ICGN) rats at the later stage. (A) Changes in the Chao1, observed species, Shannon, and Simpson indices in the sham and ICGN rats. (B) Differences in β -diversity (principal component analysis (PCoA)) based on both unweighted and weighted UniFrac between sham and ICGN rats. (C) Relative abundance at the phylum level between sham and ICGN rats (left) and the *Firmicutes* to *Bacteroidetes* (F/B) ratio (right). (D) Relative abundance at the family level between ICGN and sham rats. (E) Differential taxa between the two groups by linear discriminant analysis (LDA) effect size (LEfSe) analysis. (F) Differential genera of intestinal microbiota in sham and ICGN rats by LEfSe analysis (LDA > 3.5). (G) Genera whose relative abundances were significantly changed between the early and later stages in the sham group. (H) Genera whose relative abundances were significantly decreased in the later stage compared with the early stage in the ICGN group. (I) Genera whose relative abundances were significantly increased in the late stage compared with the early stage in the ICGN group. (J) Enriched Kyoto Encyclopedia of Genes and Genomes (KEGG) pathways at levels dominated by sham and ICGN rats, respectively. (K) Histopathological images of colon tissues by hematoxylin and eosin (HE) (top) staining and transmission electron microscopy (TEM) (bottom). The red arrow indicates the intestinal villi and the yellow arrow indicates the tight junction. (L, M) Tight junction proteins of intestinal epithelium, zonula occludens-1 (ZO-1), MUC2, occludin-1, and claudin-1 (J), and their densitometric analysis (M). (N) Concentration of lipopolysaccharide (LPS) in serum between sham and ICGN rats. * $P < 0.05$, ** $P < 0.01$, *** $P < 0.001$, and **** $P < 0.0001$ by analysis of variance (ANOVA) ($n = 10$). PC: principal component.

stage (Fig. 3E). A total of 37 biomarkers could distinguish between ICGN rats and sham at the genus level (Fig. S3); only LDA > 3.5 genus are shown in Fig. 3F. The LEfSe (LDA > 3.5) results demonstrated that the ICGN rats were mainly characterized by a higher abundance of *Allobaculum*, *Bacilli*, *Streptococcus*, *Prevotella-9*, *Blautia*, and *Lactobacillales*, whereas the sham rats primarily showed a higher enrichment of *Prevotellaceae_UCG_001*, *Turicibacter*, *Christensenellaceae*, and *Alistipes*; the relative abundances of these representative genera are shown in Fig. S4.

To better understand the changes in the gut microbiota during the early and later stages of ICGN, we screened and identified 13 genera that had the same changing trend in both the early and later stages, the names and fold-changes of which are listed in Table 1. Among them, based on LEfSe and Kruskal-Wallis statistical analyses, the relative abundances of three genera showed statistical differences both in the early and later stages, of which *Marvinbryantia* and *Allobaculum* were upregulated, while *Anaerospobacter* was downregulated (Table 1). We also performed statistical analysis of the 16S rDNA data collected at the two time points. Four genera were significantly altered in the sham group, which were considered to be influenced by aging or environmental factors (Fig. 3G). After removing these four genera, the relative abundance of 18 genera showed statistical differences between the early and later stages in the ICGN group; five genera were downregulated (Fig. 3H) and 13 were upregulated in the later stage (Fig. 3I). Among the five downregulated genera, *Lactobacillus*, which is widely accepted as a probiotic, had the highest relative abundance. The other four downregulated genera had relatively lower relative abundances, all below 0.1% of the total microbiota (Fig. 3H), and a significantly reduced relative abundance of *Odoribacter* in ICGN was also observed in the early stage (Fig. 2F). Among the 13 upregulated genera, *Marvinbryantia* and *Allobaculum* were detected again, suggesting that these two genera may play key roles in ICGN progression. This in-depth data mining provides a panoramic view to better understand the dynamic changes in the gut microbiota during ICGN progression.

To predict the possible impact of the altered gut microbiome in ICGN rats at later stages, PICRUSt analysis showed 163 altered level 3 KEGG metabolic pathways, including reduced energy metabolism, amino acid biosynthesis, and metabolism (valine, leucine, isoleucine biosynthesis, phenylalanine, tyrosine, tryptophan, and histidine) (Fig. S5). The enriched KEGG level 2 is shown in Fig. 3J. Only immune system diseases and membrane transporters were found to be enriched in the ICGN group, which is consistent with the characteristics of ICGN. Severe gut dysbiosis can disrupt the

morphological structure and function of the intestinal barrier, which was confirmed in this study. HE staining (top) and TEM (bottom) observations revealed a clear loss of microvilli and tight junctions (Fig. 3K). Western blotting demonstrated a significantly reduced expression of tight junction proteins in the intestinal epithelium (ZO-1, MUC2, claudin-1, and occludin) in the ICGN group (Figs. 3L and M). An impaired intestinal barrier can cause translocation of gut bacteria or bacterial products into the peripheral blood circulation. Using ELISA, we confirmed that the serum LPS concentration in the ICGN group was significantly higher than that in the sham group (Fig. 3N).

Taken together, these results indicate that c-BSA-induced systemic inflammation and renal dysfunction could significantly influence the composition of the gut microbiota. Furthermore, gut dysbiosis gradually deteriorated with the decline in renal function and caused a loss of the gut barrier structure.

3.4. Alteration of fecal metabolome in ICGN rats

To identify the altered fecal metabolite profile caused by ICGN, six fecal samples from each group were randomly selected, and UPLC-HDMS was used to identify untargeted metabolites in both positive and negative ion modes. A total of 4357 variables were identified, and their distribution between the two groups is shown in a heatmap (Fig. 4A) and a volcano plot (Fig. 4B). Score plots of OPLS-DA showed that ICGN rats could be clearly distinguished from sham rats (Fig. 4C). In the OPLS-DA analysis, 438 variables were found to be significantly different between the two groups, with variable importance in projection (VIP) > 1, among which 183 metabolites were upregulated and 255 were significantly downregulated. These differential metabolites were aligned to the KEGG database, and the majority were enriched in pathways associated with gut microbial metabolism; the top four were altered steroid hormone biosynthesis, tryptophan metabolism, peroxisome proliferators-activated receptors (PPAR) signaling pathway, and bile secretion (Fig. 4D).

Spearman's correlation analysis was conducted to investigate the relationship between gut flora dysbiosis and metabolomic dysregulation. The relationships between the top 20 rich differential metabolites and top 20 abundant microbial genera are listed in Fig. 4E and a correlation heatmap between the top 100 differential metabolites and gut microbiota genera is provided in Fig. S6. We found that some key genera, such as *Allobaculum* and *Marvinbryantia*, were significantly associated with several metabolites linked to the PPAR signaling pathway, linoleic acid, and tryptophan

Table 1

Significant differences in the late stage of immune-complex glomerulonephritis (ICGN) and the same trend of early changes in the microbiota.

Genera	Early stage		Later stage	
	Fold change (ICGN/sham)	P value	Fold change (ICGN/sham)	P value
Upregulated				
<i>Parabacteroides</i>	1.170929075	>0.9999	2.18592997	0.001499**
<i>Blautia</i>	1.119247514	0.3150	22.88380733	0.008151**
<i>Phascolarctobacterium</i>	1.219770644	0.6334	1.765778171	0.023342*
<i>Candidatus_Stoquefichus</i>	1.321431574	0.7193	11.90292205	0.030576*
<i>Marvinbryantia</i>	1.979180169	0.0115*	1.771297029	0.041250*
<i>Allobaculum</i>	32.86676658	0.0354*	5.736507963	0.049366*
Downregulated				
<i>Butyrivibrio</i>	0.374026069	0.1709	0.169215125	0.001474**
<i>[Eubacterium]_coprostanoligenes_group</i>	0.833749965	0.6965	0.420195108	0.003197**
<i>Clostridium_sensu_stricto_1</i>	0.586718505	0.9705	0.065581241	0.005159**
<i>Oscillibacter</i>	0.932223079	0.5288	0.450222973	0.015564*
<i>Rikenellaceae_RC9_gut_group</i>	0.550282772	0.1481	0.238830202	0.019065*
<i>Turicibacter</i>	0.860402553	0.7394	0.268282733	0.034294*
<i>Anaerospobacter</i>	0	0.0325*	0.162044902	0.047834*

* Represent compared with sham rats $P < 0.05$ and ** represent compared with sham rats $P < 0.01$.

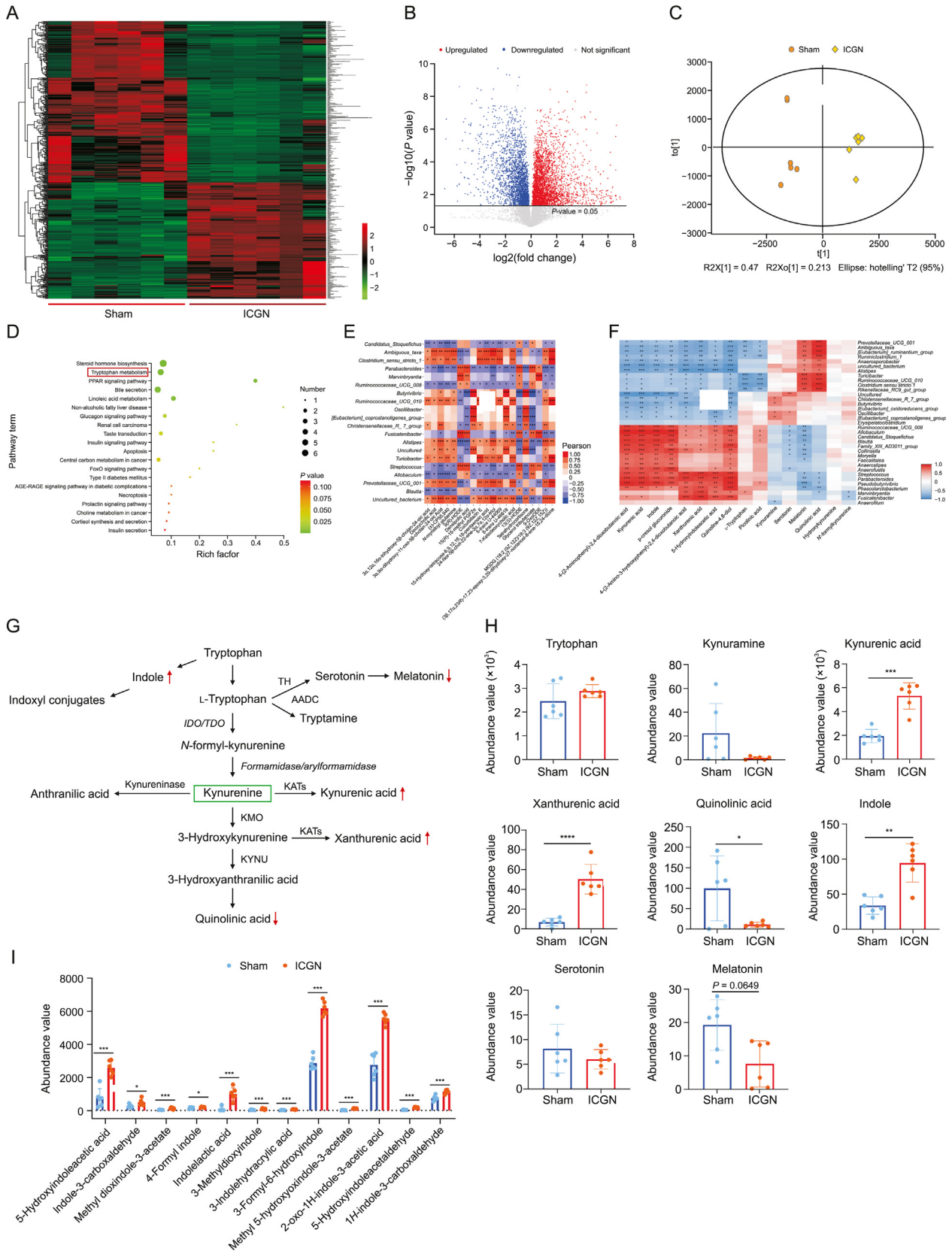


Fig. 4. Alteration of fecal metabolome in immune-complex glomerulonephritis (ICGN) rats. (A) Heatmap showing the differences in the distribution of metabolites between the model and control groups. (B) Volcano plot showing the differences in the distribution of metabolites between the model and control groups. (C) Score plots of orthogonal partial least squares-discriminant analysis (OPLS-DA) showing that ICGN rats can be clearly differentiated from the rats in the sham group. (D) Enriched Kyoto Encyclopedia of Genes and Genomes (KEGG) pathways of differential metabolites between sham and ICGN rats. (E) Spearman correlation analysis between the top 20 abundant differential genera and the top 20 abundant differential metabolites. (F) Heatmap of correlation analysis between differentially tryptophan catabolites and differential genera. (G) The three major tryptophan

metabolism, such as 13(S)-HODE, 9(R)-HODE, and quinoline. The second most abundant metabolic pathway altered by ICGN was tryptophan metabolism (Fig. 4E), which is associated with immunity and uremic toxin production. To identify the gut bacterial genera involved in the altered tryptophan metabolism, the correlation between all the detected tryptophan catabolites and bacterial genera was evaluated, as shown in a heatmap (Fig. 4F). Therefore, increased *Allobaculum*, *Blautia*, and *Parabacteroides* were found to be positively associated with indole overproduction, although these bacteria were also negatively associated with melatonin and serotonin production. There are three major tryptophan metabolism pathways, namely the kynurenine, indole, and serotonin pathways (Fig. 4G). As shown in Fig. 4H, although the total tryptophan concentration in the feces did not differ between the sham and ICGN groups, several sub-catabolic pathways were changed. As shown in Figs. 4G and H, the fecal kynurenine concentration in the ICGN group was not changed compared with the sham group ($P = 0.124$); however, its downstream kynurenic acid and xanthurenic acid were significantly increased (both $P < 0.05$), while quinolinic acid was significantly decreased, indicating that gut dysbiosis changed the kynurenine downstream catabolism pathways. In contrast, the concentrations of serotonin and melatonin showed a decreasing trend (melatonin, $P = 0.0649$) in the ICGN group, indicating that the serotonin pathway may be inhibited, suggesting that gut dysbiosis caused by ICGN may produce an adverse effect the gut-brain axis. Indole is a major tryptophan metabolite produced by the gut microbiota and a precursor of the uremic toxin indole sulfate. The indole concentration in the feces of ICGN rats was significantly higher than that in the sham control rats and tens of indoxyl conjugates (Figs. 4H and I), suggesting that the indole production pathway was markedly enhanced in the ICGN gut microbiome.

However, levels of other well-known uric toxin precursors derived from the gut microbiota, such as phenol and p-cresol, were not significantly different between the two groups. Although p-cresol glucuronide significantly accumulated in the ICGN group (5.263-fold higher changes, $P < 0.005$, ICGN vs. sham), this was likely due to lower levels of kidney excretion. Untargeted metabolomics suggested that indole may be a major uremic toxin precursor to ICGN. Short chain fatty acid, which are important beneficial metabolites of the gut microbiota, including propionic, butyric, isobutyric, valeric, and isovaleric acids, have not been examined by UPLC-HDMS because most of them are conjugated. Although acetic acid was identified, its concentration in the feces was not significantly different between the two groups; only isovaleric acid was found to be significantly increased in the ICGN group compared to that in the sham group (2.778-fold higher changes, $P = 0.004$, ICGN vs. sham).

3.5. MMF and losartan reversed dysbiosis of the gut microbiota and metabolomics dysregulation

Both losartan and MMF showed renoprotective effects by reducing albuminuria, serum creatinine, BUN, glomerulosclerosis, protein casts, and tubular injuries. Compared with the gut microbiota composition of the vehicle-treated ICGN group, both losartan and MMF seemed to slightly increase the Chao 1, observed species, Shannon indices and Simpson index, although only significant

differences were observed on Simpson index increased by MMF, which suggests that losartan and MMF have an increasing effect on the richness and diversity of the gut microbiome (Fig. 5A). As shown in Fig. 5B, the gut microbiota from the four groups were both clearly found to be $P < 0.05$ for unweighted and weighted UniFrac analyses, according to the results of PCoA analysis. These results suggest that both losartan and MMF effectively modulate and reshape the gut microbiota, albeit in different ways.

Compared with the sham group, ICGN produced 20 significantly upregulated and 19 downregulated genera. Venn analysis revealed that 17 of the 20 upregulated and 12 downregulated genera were reversed by MMF, whereas 16 of the 20 upregulated and 16 downregulated genera were reversed by losartan (Fig. 5C and Tables S1 and S2). For some well-known probiotics, such as *Bifidobacterium*, its decreased abundance was markedly reversed by MMF but not by losartan treatment (Fig. 5D). For the *Lachnospiraceae* family, which showed different trends between the early and later stages, its increased abundance was reversed only by MMF (Fig. 5E). Moreover, both MMF and losartan treatment protected the integrity of the intestinal epithelial barrier, as confirmed by pathological analysis (Fig. 5F), which also upregulated the protein levels of ZO-1, MUC, occludin, and claudin-1 (Figs. 5G and H). Meanwhile, MMF and losartan also reduced inflammation (TNF- α) and macrophage infiltration (CD68) in the colon tissues of ICGN animals; furthermore, the effect of MMF was better than that of losartan, according to the immunohistochemistry results (Figs. 5F and I).

Further metabolomic analyses revealed that treatment with MMF and losartan significantly reshaped the gut microbiota metabolite profile (Fig. 6A). Fig. 6B shows all the differential fecal metabolites with VIP > 1, which were reversed by MMF and losartan. Based on the KEGG analysis, most changes in KEGG pathways caused by ICGN (Fig. 4D) were reversed by MMF (Fig. 6C) and losartan (Fig. 6D) treatment; however, MMF seemed to be more effective in regulating the impaired gut metabolomics, both in the number of reversed metabolites and decreasing the extent of indoxyl uremic toxins (Fig. 6E). Meanwhile, in terms of the effects of MMF and losartan on other tryptophan catabolites, MMF was found to be more sensitive and effective on regulating tryptophan metabolism, and could significantly reverse the changing trend of indole, kynurenic acid, xanthurenic acid and serotonin; however, losartan treatment significantly increased the melatonin concentration in the feces more than MMF (Fig. 6F).

3.6. FMT does not ameliorate albuminuria and declined renal function in ICGN rats

Since FMT experiments are considered as the best way to determine the effects of drugs on the gut microbiota modulation, we performed FMT using fecal samples from sham (R-Sham), ICGN-vehicle (R-ICGN), ICGN-MMF (R-MMF), and ICGN-losartan-treated (R-Losartan) donor rats. During the continuous gavage of fecal contents, c-BSA was intravenously administered every two days for four weeks. Then, the intestinal bacteria were evaluated after fecal bacterial transplantation. A total of 3769 OTUs were detected, 139 of which were shared (Fig. 7A).

With regards to α -diversity, the reduced richness of microbiota flora observed in the R-ICGN group was found to be partly reversed in the donor groups of sham and MMF rats by FMT (Fig. 7B),

metabolic pathways. (H) Metabolites with significant changes in the tryptophan metabolism pathway between the sham and ICGN groups ($n = 6$). (I) Comparison of the abundance values of indoxyl conjugates derived from tryptophan metabolism ($n = 6$). * $P < 0.05$, ** $P < 0.01$, *** $P < 0.001$, and **** $P < 0.0001$ by analysis of variance (ANOVA) ($n = 10$). PPAR: peroxisome proliferators-activated receptors; FoxO: Forkhead box O; ARE-RAGE: advanced glycation end-products-receptor of advanced glycation endproducts; CP 55,940: 5-(1,1-dimethylheptyl)-2-[5-hydroxy-2-(3-hydroxypropyl)cyclohexyl]phenol; HODE: hydroxy-10E,12Z-octadecadienoic acid; PGF: prostaglandin F; OxoODE: oxo-10,12-octadecadienoic acid; MGDG: monogalactosyldiacylglycerol; TH: tyrosine hydroxylase; AADC: aromatic L-amino acid decarboxylase; IDO/TDO: indoleamine 2,3-dioxygenase/tryptophan 2,3-dioxygenase gene; KATs: K(lysine) acetyltransferase; KMO: kynurenine 3-monooxygenase; KYNU: kynureninase.

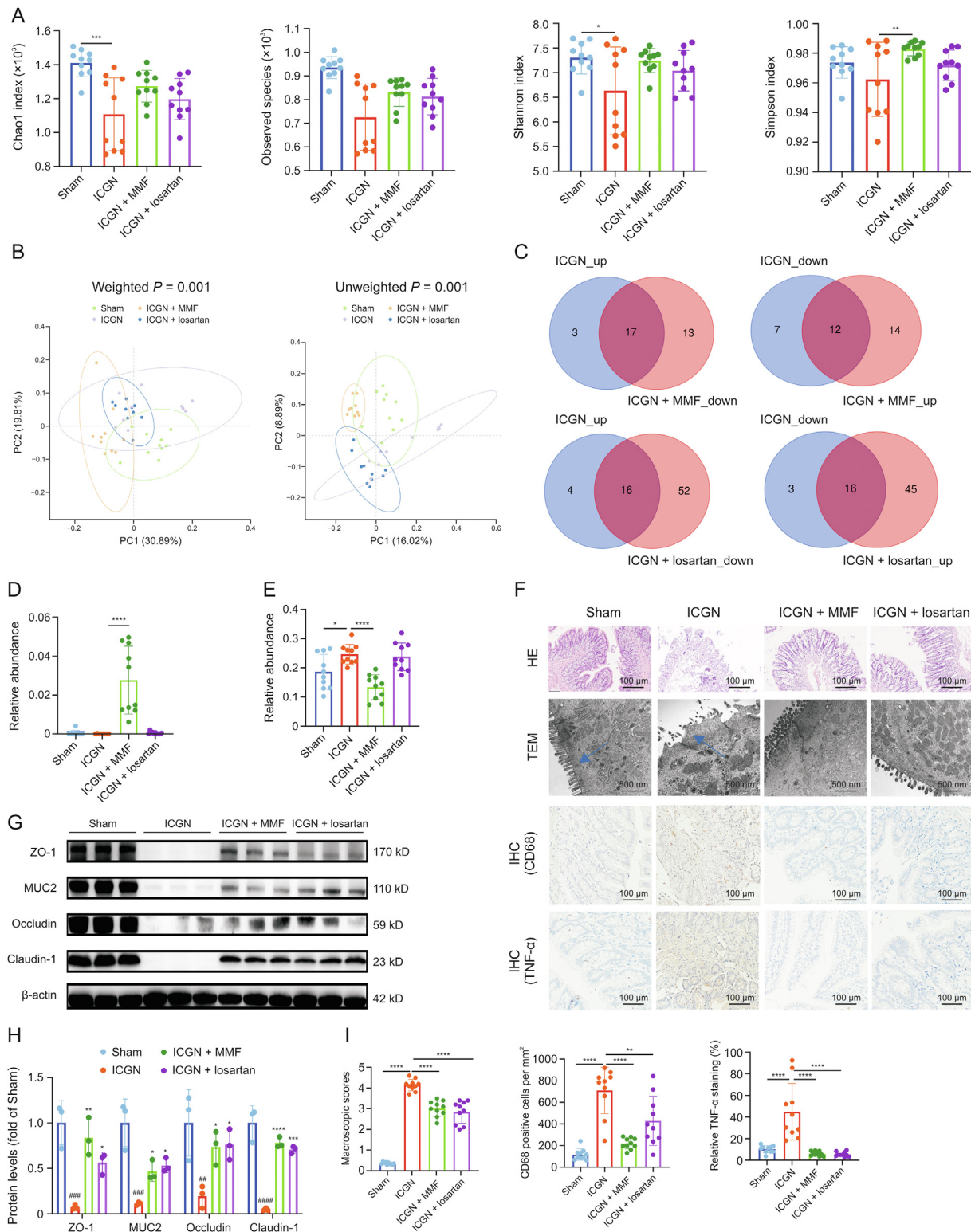


Fig. 5. Modulation of gut microbiota by treatment with mycophenolate mofetil (MMF) and losartan. (A) Effects of MMF and losartan on Chao1, observed species, Shannon, and Simpson indices. (B) The effects of MMF and losartan on gut microbiota were analyzed by unweighted and weighted principal component analysis (PCoA) analysis. (C) Venn-diagrams showing the number of differentially genera in the immune-complex glomerulonephritis (ICGN) rats that were reversed by MMF and losartan treatment. (D) Effects of MMF and losartan intervention on intestinal probiotic *Bifidobacterium*. (E) Effects of MMF and losartan intervention on *Lachnospiraceae* family. (F) Results of hematoxylin and eosin (HE) staining, transmission electron microscopy (TEM), and immunohistochemistry (IHC). The blue arrow indicates the intestinal villi. (G, H) Western blot results of tight junction proteins of intestinal epithelium, zonula occludens-1 (ZO-1), occludin-1, claudin-1, and MUC2 (G) and their densitometric analysis (* represents compared with sham rats and * represents compared with ICGN rats) (H). (I) The quantitation analysis of Fig. 5F: HE and TEM (left); cluster of differentiation 68 (CD68; IHC) (middle); and tumor necrosis factor- α (TNF- α ; IHC) (right). * $P < 0.05$, ** $P < 0.01$, *** $P < 0.001$, and **** $P < 0.0001$ by analysis of variance (ANOVA) ($n = 10$). PC: principal component.

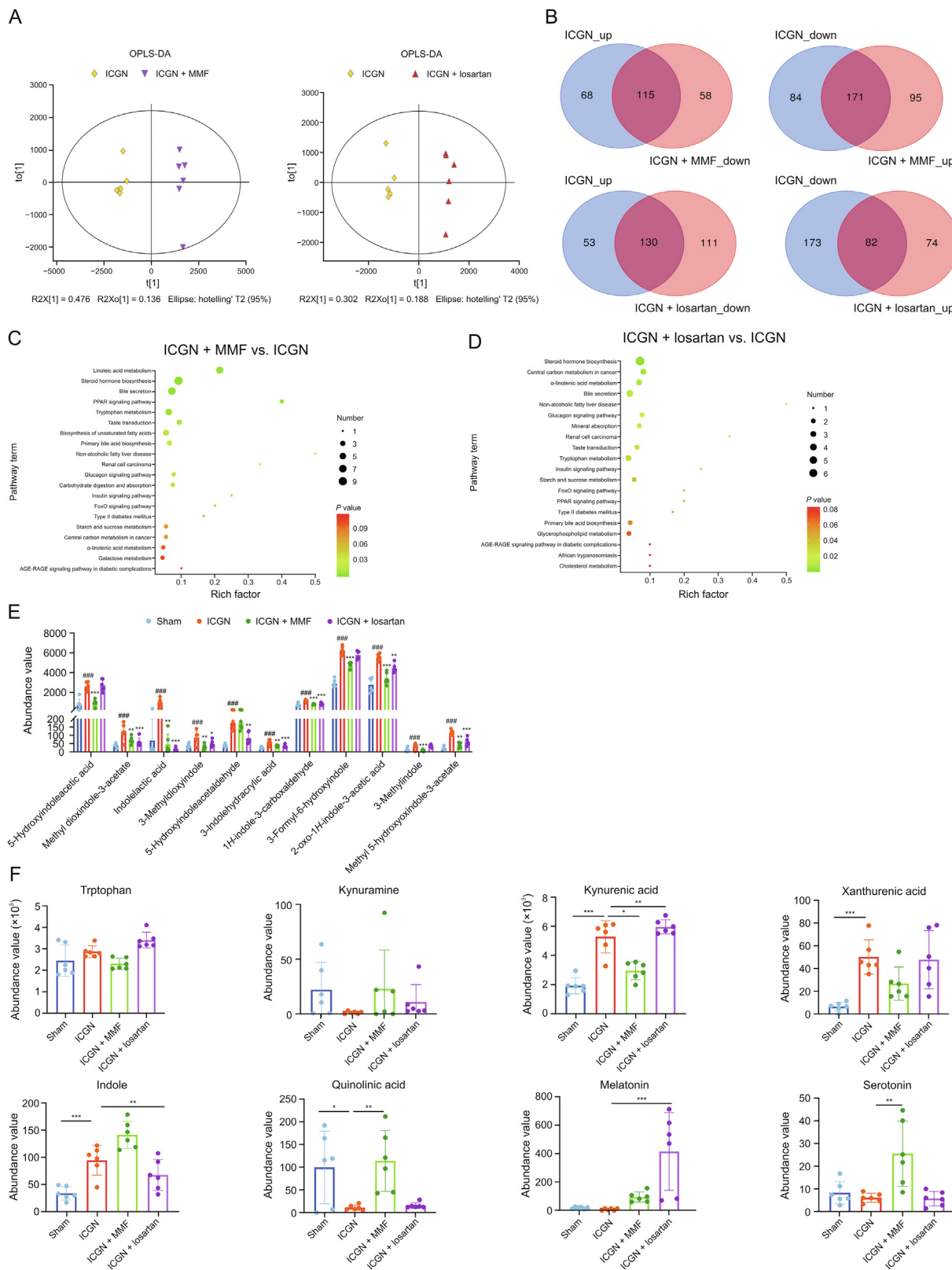


Fig. 6. Metabolomics altered by mycophenolate mofetil (MMF) and losartan treatment. (A) Differences in metabolite composition between immune-complex glomerulonephritis (ICGN), MMF, and losartan groups. (B) The number of differential metabolites reversed by losartan and MMF treatment by Venn analysis. (C, D) Kyoto Encyclopedia of Genes and Genomes (KEGG) pathways enriched by differential metabolites reversed by MMF (C) and losartan (D) treatments compared with the ICGN group. (E) Fecal concentration of nephrotoxic indoxyl conjugates in sham, ICGN, MMF, and losartan treatment groups (*represents compared with sham rats and * represents compared with ICGN rats) ($n = 6$). (F) Distribution of tryptophan derived catabolites ($n = 6$). * $P < 0.05$, ** $P < 0.01$, *** $P < 0.001$, and **** $P < 0.0001$ by analysis of variance (ANOVA) ($n = 10$). OPLS-DA: orthogonal partial least squares-discriminant analysis; PPAR: peroxisome proliferators-activated receptors; FoxO: Forkhead box O; ARE-RAGE: advanced glycation end-products-receptor of advanced glycation endproducts.

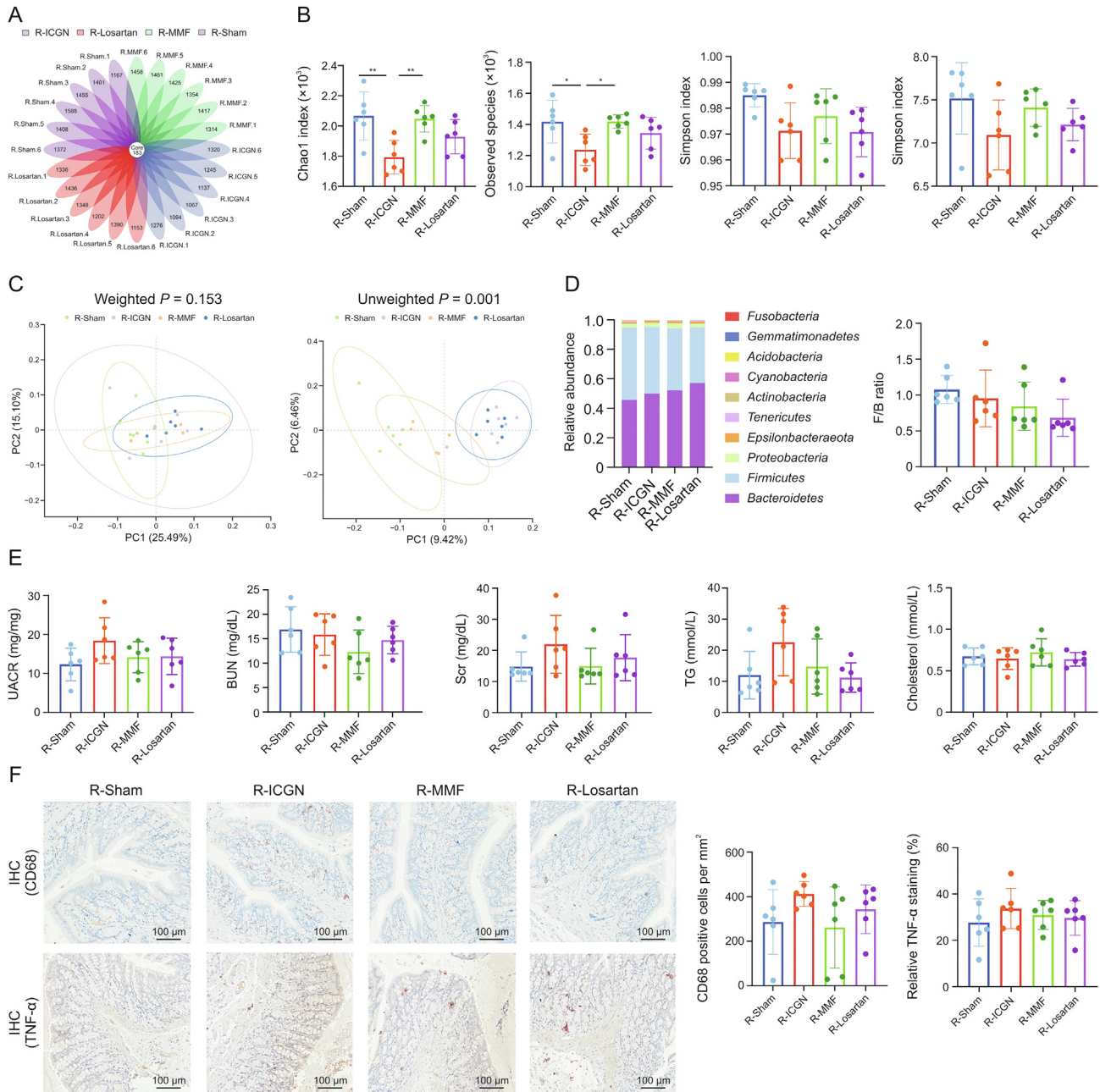


Fig. 7. Fecal microbiota transplantation (FMT) ameliorates the gut dysbiosis induced by immune-complex glomerulonephritis (ICGN) but does not attenuate renal impairments. (A) A total of 3769 operational units (OTUs) were detected, 139 of which shared the same OTUs among the four experimental groups. (B) FMT from sham and mycophenolate mofetil (MMF) donor rats increased the richness of the gut microbiota (Chao1 and observed species indices) but not the diversity (Shannon and Simpson indices). $^*P < 0.05$, $^{**}P < 0.01$, and $^{***}P < 0.001$ compared with ICGN-vehicle (R-ICGN). (C) β -diversity analysis showed that the species composition of each group was significantly different and could be distinguished clearly. (D) The relative abundance of the phylum levels among the four groups (left) and *Firmicutes* to *Bacteroidetes* (F/B) ratio (right). (E) No significant difference was observed in terms of blood urine nitrogen (BUN), serum creatinine (Scr), triglyceride (TG), and serum total cholesterol among the four groups. (F) FMT slightly reduced inflammation and macrophage infiltration in colon tissues by immunohistochemical staining using anti-cluster of differentiation 68 (CD68) and anti-tumor necrosis factor- α (TNF- α) antibodies. $^*P < 0.05$, $^{**}P < 0.01$, $^{***}P < 0.001$, and $^{****}P < 0.0001$ by analysis of variance (ANOVA) ($n = 6$). R-Losartan: ICGN-losartan-treated; R-MMF: ICGN-MMF; R-Sham: fecal samples from sham; PC: principal component; UACR: urine albumin-to-creatinine ratio; IHC: immunohistochemistry.

including the Chao1, observed species, and Simpson and Shannon indices, although the diversity indices, including Shannon and Simpson indices, showed no statistical differences among the four groups (Fig. 7B). By contrast, β -diversity analysis showed that the bacterial composition was significantly different among the four groups and could be completely distinguished (Fig. 7C), demonstrating the success of FMT.

By analyzing the taxonomic composition between groups at the phylum level and calculating the F/B ratio, we found that the F/B

ratio in the R-MMF and R-Losartan groups was lower than that in the R-ICGN group after fecal bacterial transplantation, although the difference was not statistically significant (Fig. 7D). However, upon analyzing kidney function, the FMT from sham, MMF, or losartan-treated donor rats did not ameliorate BUN, Scr, TG, or serum total cholesterol, which suggests that the modulation of the gut microbiota only partially contributed to a beneficial renal effect (Fig. 7E). Meanwhile, by immunohistochemistry, FMT from the MMF and losartan donor rats appeared to slightly reduce inflammation (TNF-

α) and macrophage infiltration (CD68) in the colon tissues, although no statistical difference was observed (Fig. 7F).

4. Discussion

ICGN is an immune-mediated disease that can lead to chronic inflammation of the glomeruli and the kidney tubular interstitium [33]. Overactivation of immune function can directly or indirectly induce ICGN, leading to loss of kidney function [34]. CKD has been the fastest-growing cause of kidney-related deaths in recent years, as it tends to develop into late-stage renal failure [34], and ICGN accounts for approximately 20% of CKD cases [35]. The gut microbiome is considered as a giant bioreactor of the human body, interacting bidirectionally with the host [36]. Recently, increasing evidence has indicated that the gut microbiota is closely involved in the pathogenesis of ICGN [37,38].

Firmicutes, *Bacteroidetes*, *Proteobacteria*, and *Actinobacteria* are the dominant bacterial phyla in the rat microbiome. F/B is considered as an important index of gut composition, and, as expected, the ICGN ratio gradually increases the F/B ratio. To better understand the changes in the gut microbiota during the early and later stages of ICGN, 18 genera with statistical differences between the early and later stages in the ICGN group were identified. Among these, *Marvinbryantia* and *Allobaculum* shared the same trend between early and later stages, and also showed a significant difference between ICGN and sham even at the early stage. *Marvinbryantia* and *Allobaculum* were both upregulated, had a relatively high abundance in the gut microbiome, and were key genera involved in the progression of ICGN. According to the literature, an abundance of *Allobaculum* has been associated with inflammation and renal failure in diabetic nephropathy [39,40], though the underlying mechanisms remains unclear. Although reports on the association between *Marvinbryantia* and kidney disease are scarce, several publications suggest that *Marvinbryantia* may play an important role in host immune activity, such as the response to PD-1 antibody in patients with cancer [41,42]. Overall, the detailed mechanisms by which *Marvinbryantia* and *Allobaculum* regulate ICGN, as well as other significantly altered genera during ICGN progression, require further study.

The progressive loss of kidney function and systemic chronic inflammation in ICGN contribute to profound changes in the gut microbiome and microbiome-derived metabolites. The gut microbiota are mostly involved in amino acid metabolism, energy metabolism, nervous, endocrine, immune, and digestive systems, lipid metabolism, and carbohydrate metabolism [43]. Altered microbial-derived metabolites are closely associated with inflammation and fatty acid dysregulation, the dominant pathways of which are tryptophan and linoleic acid metabolism. Significant changes in the abundance of 39 bacterial genera and 438 differential metabolites were observed in ICGN rats compared to sham controls, highlighting the significant impact of ICGN on the gut microbiome and its role in dysregulated metabolites. Both MMF and losartan can reshape the eubiosis of the gut microbiota, increase the richness and diversity of the gut microbiome, and reverse almost half of the altered bacterial species.

In the present study, the most abundant gut microbiota family was *Lachnospiraceae* in the host rats. The main microbial pathways associated with *Lachnospiraceae* include the biosynthesis of acetate and butyrate and the metabolic pathways of aromatic amino acids involved in the biosynthesis of indole-propionic acid, indole, phenol, and p-cresol [44]. Notably, in this study, the relative abundance of *Lachnospiraceae* was found to differ between the early and later stages. One possible explanation is that at the early stage, the change in the gut microbiota was

mainly regulated by the host acute immune reaction but not declined kidney function. However, in the later stage, the gut microbiota was mainly influenced by kidney function loss due to the amount of uremic toxins accumulated in the colon, causing sharp changes in the colon microenvironment. Therefore, we hypothesized that the relative abundance of the *Lachnospiraceae* family decreased due to acute inflammation caused by c-BSA challenge in the early stage, which is similar to the decreased *Lachnospiraceae* observed in inflammatory bowel disease [45]. However, in later stages, similar to most CKD studies, the relative abundance of *Lachnospiraceae* was found to increase significantly compared to that in the healthy controls [46], which is consistent with the results reported herein. As shown in Fig. 5E, MMF treatment significantly reduced the relative abundance of *Lachnospiraceae*, but not of losartan, suggesting that *Lachnospiraceae* is prone to be influenced by the immune status in the colon's microenvironment.

Belonging to the *Lachnospiraceae* family, *Blautia* was markedly elevated in the ICGN rats at the later stage, providing additional evidence, similar to the results reported by Zeng et al. [47], suggesting that *Blautia* is more influenced by declined renal function. In addition, increased *Blautia* has been previously reported to be associated with an early decline in renal function (estimated glomerular filtration rate decline) in a large cohort of patients with minimal renal dysfunction [48]. Vancomycin administration in patients with end-stage renal disease has been shown to significantly reduce *Blautia* and the serum IS and p-CS levels on day 7 [49]. Herein, the relative abundance of *Blautia* was also found to be positively correlated with indole, p-cresol glucuronide, and kynurenic acid by Spearman correlation analysis.

In this study, KEGG analysis of fecal differential metabolites showed that tryptophan metabolism was the second most activated pathway in the gut microbiota of ICGN rats, indicating the importance of tryptophan metabolism in ICGN. Tryptophan is the biosynthetic precursor of many metabolites. There are three metabolic pathways for tryptophan in the human gut: i) in intestinal epithelial cells and immune cells, approximately 90% of tryptophan is metabolized to kynurenine through indoleamine 2,3-dioxygenase 1, which is the kynurenine acid pathway [50]; ii) in the intestinal cavity, the gut microbiota directly metabolizes 4%–6% of tryptophan into indole and its indoxyl derivatives; and iii) 3% of tryptophan in intestinal chromaffin cells is metabolized to 5-hydroxytryptamine through tryptophan hydroxylase 1, which is the serotonin pathway, producing over 90% of total serotonin [17]. Herein, dysbiosis caused by ICGN significantly upregulated the indole production pathway and downregulated the serotonin-melatonin pathway. Although kynurenine concentration was not significantly changed in ICGN animals, the production of KynA and xanthurenic acid increased, and quinolinic acid decreased, indicating that the sub-metabolic pathways had been altered.

Tryptophan plays an important role in the balance between intestinal immune tolerance and the maintenance of the gut microbiota. The gut microbiota affects the host immune system by regulating tryptophan metabolism. Although some studies have suggested that indole and its derivatives can enhance intestinal barrier function by increasing the expression of tight junction proteins [51] and reducing inflammation through aromatic hydrocarbon receptor-mediated regulation of intestinal immunity [52], their toxic effects are dominant and widely accepted. In the c-BSA-induced ICGN model, indole and its conjugates only increased uremic toxins compared to the sham control (phenol, cresol, and trimethylamine *N*-oxide did not change), suggesting that altered tryptophan metabolism mediated by the gut microbiota may play a key role in the progression of ICGN. Some studies claim that there is

no association between indoxyl sulfate and incident CKD [53], but for immune-mediated ICGN, tryptophan-indole metabolism seems to be different. In many clinical studies, the concentration of fecal indole in CKD patients did not change compared with that in healthy controls [54], suggesting that immune-mediated CKD may have a unique gut microbiota-changing pattern, which warrants further study. In addition, animal models may have characteristics different from those of humans; therefore, more attention must be paid to these differences. In contrast, reducing indole production by targeting the gut microbiota has been considered as a strategy to alleviate CKD, although its clinical effects have yet to be verified [8]. Tryptophan metabolites serve as a bridge between the microbiota and host, achieving the integration of gut microbiota and drug targets and bringing new opportunities and possibilities for the application and transformation of gut microbiota-related research in the field of drug targets.

Lastly, with regards to the effects of losartan and MMF on gut dysbiosis in patients with ICGN, an analysis of the changes in intestinal bacteria and their metabolites may provide novel perspectives to explain the efficacy of these two drugs in CKD treatment. Dysbiosis of the gut microbiota and dysregulated fecal metabolites in ICGN were found to be partially reversed by losartan and MMF treatment, among which MMF showed a slightly better performance, reversing 286 differential metabolites compared to 212 differential metabolites reversed by losartan. More importantly, the reducing effect of MMF on indole and indoxyl conjugates of MMF was much greater than that of losartan. As for other tryptophan catabolites, MMF also has a stronger effect than losartan, as it can significantly change the fecal concentrations of kynurenic acid, serotonin, and quinolinic acid, in contrast to losartan.

In addition, the enhanced permeability of the intestinal barrier, allowing the passage of endotoxins and other bacterial products into the blood, was also demonstrated herein, as well as in almost all CKD cases [55]. Endotoxemia is a common feature of CKD and is one of the causes of systemic inflammation, which affects the majority of patients with CKD [56]. The gut epithelium is an efficient barrier that prevents the translocation of pathogens and the absorption of LPS. LPS can activate Toll-like receptor-4 (TLR4), leading to the production of numerous pro-inflammatory cytokines and low-grade systemic inflammation [57]. LPS is also an important indicator of intestinal barrier damage and inflammation. Thus, as expected, ICGN rats showed significantly higher LPS values and impaired gut permeability. As expected, both MMF and losartan treatment increased the tight junctions of the intestinal barrier and reduced the translocation of LPS into circulation.

FMT refers to the transplantation of functional flora in feces into the intestines of subjects to reconstruct new intestinal flora and treat intestinal diseases. It is often used to treat severe inflammation and metabolic disorders. Herein, FMT was used to evaluate the protective effects of MMF and losartan on the kidneys. As expected, the α -diversity index in MMF- and losartan-treated rats was alleviated after FMT, with a corresponding decrease in the F/B ratio. Although these parameters indicate an improvement of gut dysbiosis, renal function loss in ICGN rats was not slowed by FMT, suggesting that the modulation of the gut microbiota alone is not enough to improve renal injury.

Overall, this study provides an overview of the dynamic changes in the intestinal microbiome and metabolome in c-BSA-induced ICGN, highlighting the regulatory effect of losartan and MMF on the microbiome and metabolome. In addition, FMT was conducted and no improvement in renal function was observed, suggesting that whether the modulation of gut dysbiosis is beneficial for kidney injury requires further study.

5. Conclusion

In the present study, we confirmed the intestinal microbiota imbalance and metabolomic changes related to ICGN induced by c-BSA. Our findings elucidate a novel mechanism underlying the therapeutic effect of losartan and MMF in improving gut microbial dysbiosis and associated metabolomic disorders, which partially contributes to their renoprotective effects against ICGN. In addition, FMT was found to improve gut dysbiosis by decreasing the F/B ratio. However, renal function and albuminuria were not improved by FMT treatment, suggesting that the regulation of intestinal dysbiosis is beneficial to kidney injury, although this will require further study.

CRedit author statement

Wenyang Shi and Zhaojun Li: Writing - Original draft preparation, Data curation, Formal analysis; Weida Wang and Xikun Liu: Investigation, Validation; Haijie Wu and Xiaoguang Chen: Validation; Xunrong Zhou and Sen Zhang: Writing - Reviewing and Editing, Conceptualization, Methodology, Supervision.

Declaration of competing interest

The authors declare that there are no conflicts of interest.

Acknowledgments

The authors acknowledge the funds by the Chinese Academy of Medical Sciences Innovation Fund for Medical Sciences (CIFMS), China (Grant No.: 2022-I2M-1-014), the National Natural Science Foundation of China (Grant No.: 82293684), Beijing Natural Science Foundation, China (Grant No.: L232084), and the National Key R&D Program of China (Grant No.: 2022YFA0806400).

Appendix A. Supplementary data

Supplementary data to this article can be found online at <https://doi.org/10.1016/j.jpha.2023.12.021>.

References

- [1] C. Meyer-Schwesinger, S. Dehde, P. Klug, et al., Nephrotic syndrome and subepithelial deposits in a mouse model of immune-mediated anti-podocyte glomerulonephritis, *J. Immunol.* 187 (2011) 3218–3229.
- [2] J.M. Thurman, M. Le Quintrec, Targeting the complement cascade: Novel treatments coming down the Pike, *Kidney Int.* 90 (2016) 746–752.
- [3] G.R. Valiente, A. Munir, M.L. Hart, et al., Gut dysbiosis is associated with acceleration of lupus nephritis, *Sci. Rep.* 12 (2022), 152.
- [4] Q. Mu, H. Zhang, X. Liao, et al., Control of lupus nephritis by changes of gut microbiota, *Microbiome* 5 (2017), 73.
- [5] S. Zhang, W. Wang, L. Yan, et al., Nicousamide attenuates renal dysfunction and glomerular injury in remnant kidneys by inhibiting TGF- β 1 internalisation and renin activity, *Eur. J. Pharmacol.* 845 (2019) 74–84.
- [6] I.W. Wu, C. Lin, L.C. Chang, et al., Gut microbiota as diagnostic tools for mirroring disease progression and circulating nephrotoxin levels in chronic kidney disease: Discovery and validation study, *Int. J. Biol. Sci.* 16 (2020) 420–434.
- [7] T. Gryp, K. De Paep, R. Vanholder, et al., Gut microbiota generation of protein-bound uremic toxins and related metabolites is not altered at different stages of chronic kidney disease, *Kidney Int.* 97 (2020) 1230–1242.
- [8] A.M. Madella, J. van Bergenhengouwen, J. Garssen, et al., Microbial-derived tryptophan catabolites, kidney disease and gut inflammation, *Toxins* 14 (2022), 645.
- [9] R. Yacoub, G.N. Nadkarni, D.I. McSkimming, et al., Fecal microbiota analysis of polycystic kidney disease patients according to renal function: A pilot study, *Exp. Biol. Med.* (Maywood) 244 (2019) 505–513.
- [10] D. Azzouz, A. Omarbekova, A. Heguy, et al., Lupus nephritis is linked to disease-activity associated expansions and immunity to a gut commensal, *Ann. Rheum. Dis.* 78 (2019) 947–956.
- [11] H. Wu, B. Jia, X. Zhao, et al., Pathophysiology and system biology of rat c-BSA induced immune complex glomerulonephritis and pathway comparison with

- human gene sequencing data, *Int. Immunopharmacol.* 109 (2022), 108891.
- [12] P.N. Furness, D.R. Turner, Chronic serum sickness glomerulonephritis: Passive immunisation inhibits the removal of glomerular antigen and electron dense deposits, *Virchows Arch. A Pathol. Anat. Histopathol.* 413 (1988) 551–553.
- [13] K. Joh, S. Aizawa, K. Ohkawa, et al., Selective planting of cationized, haptenized ovalbumin on the rat tubular basement membrane, *Virchows Arch.* 424 (1994) 587–591.
- [14] M.C. Villarreal, M. Hidalgo, A. Jimeno, Mycophenolate mofetil: An update, *Drugs Today* 45 (2009) 521–532.
- [15] P. Li, H. Lin, Z. Ni, et al., Efficacy and safety of *Abelmoschus manihot* for IgA nephropathy: A multicenter randomized clinical trial, *Phytomedicine* 76 (2020), 153231.
- [16] V. Sepe, C. Libetta, M.G. Giuliano, et al., Mycophenolate mofetil in primary glomerulopathies, *Kidney Int.* 73 (2008) 154–162.
- [17] M. Platten, E.A.A. Nollen, U.F. Röhrig, et al., Tryptophan metabolism as a common therapeutic target in cancer, neurodegeneration and beyond, *Nat. Rev. Drug Discov.* 18 (2019) 379–401.
- [18] J. Zou, X. Zhou, Y. Ma, et al., Losartan ameliorates renal interstitial fibrosis through metabolic pathway and Smurfs-TGF- β /Smad, *Biomed. Pharmacother.* 149 (2022), 112931.
- [19] H. Wang, W. Fu, Z. Jin, et al., Advanced IgA nephropathy with impaired renal function benefits from losartan treatment in rats, *Ren. Fail.* 35 (2013) 812–818.
- [20] I. Robles-Vera, M. Toral, N. de la Visitación, et al., Changes to the gut microbiota induced by losartan contributes to its antihypertensive effects, *Br. J. Pharmacol.* 177 (2020) 2006–2023.
- [21] S. Zhang, H. Xin, Y. Li, et al., Skimmin, a coumarin from *Hydrangea paniculata*, slows down the progression of membranous glomerulonephritis by anti-inflammatory effects and inhibiting immune complex deposition, *Evid. Based Complement. Alternat. Med.* 2013 (2013), 819296.
- [22] S. Zhang, J. Ma, L. Sheng, et al., Total coumarins from *Hydrangea paniculata* show renal protective effects in lipopolysaccharide-induced acute kidney injury via anti-inflammatory and antioxidant activities, *Front. Pharmacol.* 8 (2017), 872.
- [23] W. Wang, Z. Li, Y. Chen, et al., Prediction value of serum NGAL in the diagnosis and prognosis of experimental acute and chronic kidney injuries, *Bio-molecules* 10 (2020), 981.
- [24] M. Eddouks, D. Chattopadhyay, V. De Feo, et al., Medicinal plants in the prevention and treatment of chronic diseases 2013, *Evid. Based Complement. Alternat. Med.* 2014 (2014), 180981.
- [25] C. Huang, J. Dong, X. Jin, et al., Intestinal anti-inflammatory effects of fuzi-ganjiang herb pair against DSS-induced ulcerative colitis in mice, *J. Ethnopharmacol.* 261 (2020), 112951.
- [26] S. Zhang, W. Wang, J. Ma, et al., Coumarin glycosides from *Hydrangea paniculata* slow down the progression of diabetic nephropathy by targeting Nrf2 anti-oxidation and smad2/3-mediated profibrosis, *Phytomedicine* 57 (2019) 385–395.
- [27] S. Zhang, D. Wang, N. Xue, et al., Nicousamide protects kidney podocyte by inhibiting the TGF β receptor II phosphorylation and AGE-RAGE signaling, *Am. J. Transl. Res.* 9 (2017) 115–125.
- [28] L.F. Gomez-Arango, H.L. Barrett, S.A. Wilkinson, et al., Low dietary fiber intake increases *Collinsella* abundance in the gut microbiota of overweight and obese pregnant women, *Gut Microbes* 9 (2018) 189–201.
- [29] Y. Feng, G. Cao, D. Chen, et al., Microbiome-metabolomics reveals gut microbiota associated with glycine-conjugated metabolites and polyamine metabolism in chronic kidney disease, *Cell. Mol. Life Sci.* 76 (2019) 4961–4978.
- [30] D. Chen, G. Cao, H. Chen, et al., Identification of serum metabolites associating with chronic kidney disease progression and anti-fibrotic effect of 5-methoxytryptophan, *Nat. Commun.* 10 (2019), 1476.
- [31] C.J. Chang, C. Lin, C.C. Lu, et al., *Ganoderma lucidum* reduces obesity in mice by modulating the composition of the gut microbiota, *Nat. Commun.* 6 (2015), 7489.
- [32] S. Dong, Q. Liu, X. Zhou, et al., Effects of losartan, atorvastatin, and aspirin on blood pressure and gut microbiota in spontaneously hypertensive rats, *Molecules* 28 (2023), 612.
- [33] S.J. Chadban, R.C. Atkins, Glomerulonephritis, *Lancet* 365 (2005) 1797–1806.
- [34] A.C. Webster, E.V. Nagler, R.L. Morton, et al., Chronic kidney disease, *Lancet* 389 (2017) 1238–1252.
- [35] B. Liu, Y. Cao, D. Wang, et al., Zhen-wu-Tang induced mitophagy to protect mitochondrial function in chronic glomerulonephritis via PI3K/AKT/mTOR and AMPK pathways, *Front. Pharmacol.* 12 (2021), 777670.
- [36] M. Chi, K. Ma, J. Wang, et al., The immunomodulatory effect of the gut microbiota in kidney disease, *J. Immunol. Res.* 2021 (2021), 5516035.
- [37] A. Rutsch, J.B. Kantsjö, F. Ronchi, The gut-brain axis: How microbiota and host inflammasome influence brain physiology and pathology, *Front. Immunol.* 11 (2020), 604179.
- [38] Y. Zhao, Y. Liu, S. Li, et al., Role of lung and gut microbiota on lung cancer pathogenesis, *J. Cancer Res. Clin. Oncol.* 147 (2021) 2177–2186.
- [39] P. Wang, T. Wang, X. Zheng, et al., Gut microbiota, key to unlocking the door of diabetic kidney disease, *Nephrology (Carlton)* 26 (2021) 641–649.
- [40] A. Zaky, S.J. Glastras, M.Y.W. Wong, et al., The role of the gut microbiome in diabetes and obesity-related kidney disease, *Int. J. Mol. Sci.* 22 (2021) 9641.
- [41] R. Suraya, T. Nagano, K. Kobayashi, et al., Microbiome as a target for cancer therapy, *Integr. Cancer Ther.* 19 (2020), 1534735420920721.
- [42] R.C. Newsome, R.Z. Gharaibeh, C.M. Pierce, et al., Interaction of bacterial Genera associated with therapeutic response to immune checkpoint PD-1 blockade in a United States cohort, *Genome Med* 14 (2022), 35.
- [43] R. Chen, J. Wang, R. Zhan, et al., Fecal metabolomics combined with 16S rRNA gene sequencing to analyze the changes of gut microbiota in rats with kidney-Yang deficiency syndrome and the intervention effect of You-Gui pill, *J. Ethnopharmacol.* 244 (2019), 112139.
- [44] M. Vacca, G. Celano, F.M. Calabrese, et al., The controversial role of human gut Lachnospiraceae, *Microorganisms* 8 (2020), 573.
- [45] K. Sasaki, J. Inoue, D. Sasaki, et al., Construction of a model culture system of human colonic microbiota to detect decreased Lachnospiraceae abundance and butyrogenesis in the feces of ulcerative colitis patients, *Biotechnol. J.* 14 (2019), e1800555.
- [46] J. Yang, S.Y. Lim, Y.S. Ko, et al., Intestinal barrier disruption and dysregulated mucosal immunity contribute to kidney fibrosis in chronic kidney disease, *Nephrol. Dial. Transplant* 34 (2019) 419–428.
- [47] Y. Zeng, Z. Dai, F. Lu, et al., Emodin via colonic irrigation modulates gut microbiota and reduces uremic toxins in rats with chronic kidney disease, *Oncotarget* 7 (2016) 17468–17478.
- [48] C. Barrios, M. Beaumont, T. Pallister, et al., Gut-microbiota-metabolite axis in early renal function decline, *PLoS One* 10 (2015), e0134311.
- [49] L. Nazzari, J. Roberts, P. Singh, et al., Microbiome perturbation by oral vancomycin reduces plasma concentration of two gut-derived uremic solutes, indoxyl sulfate and p-cresyl sulfate, in end-stage renal disease, *Nephrol. Dial. Transplant* 32 (2017) 1809–1817.
- [50] M.T. Pallotta, S. Rossini, C. Suvieri, et al., Indoleamine 2, 3-dioxygenase 1 (IDO1): An up-to-date overview of an eclectic immunoregulatory enzyme, *FEBS J* 289 (2022) 6099–6118.
- [51] H.M. Roager, T.R. Licht, Microbial tryptophan catabolites in health and disease, *Nat. Commun.* 9 (2018), 3294.
- [52] J. Liu, H. Miao, D. Deng, et al., Gut microbiota-derived tryptophan metabolism mediates renal fibrosis by aryl hydrocarbon receptor signaling activation, *Cell. Mol. Life Sci.* 78 (2021) 909–922.
- [53] S. Kalim, E.P. Rhee, An overview of renal metabolomics, *Kidney Int.* 91 (2017) 61–69.
- [54] C.Y. Yang, T. Chen, W. Lu, et al., Synbiotics alleviate the gut indole load and dysbiosis in chronic kidney disease, *Cells* 10 (2021), 114.
- [55] S. Cigarran Guldris, E. González Parra, A. Cases Amenós, Gut microbiota in chronic kidney disease, *Nefrología* 37 (2017) 9–19.
- [56] J. Wong, E. Vilar, K. Farrington, Endotoxemia in end-stage kidney disease, *Semin. Dial.* 28 (2015) 59–67.
- [57] S. Mohammad, C. Thiemermann, Role of metabolic endotoxemia in systemic inflammation and potential interventions, *Front. Immunol.* 11 (2020), 594150.